Characterization of the H2O+CO2 continuum within the infrared transparency windows

H. Fleurbaey, A. Campargue, Y. Carreira Mendès D Silva, R. Grilli, S. Kassi, Didier Mondelain

Characterization of the H_2O+CO_2 continuum within the infrared transparency windows

H. Fleurbaey[a], A. Campargue[a], Y. Carreira Mendès Da Silva[a], R. Grilli[b], S. Kassi[a], D. Mondelain[a,*]

[a] *Univ. Grenoble Alpes, CNRS, LIPhy, 38000 Grenoble, France*
[b] *Univ. Grenoble Alpes, CNRS, IRD, Grenoble INP, IGE, 38000 Grenoble, France*

[*] Corresponding author: didier.mondelain@univ-grenoble-alpes.fr; LIPhy, Bat. E, 140 rue de la Physique, 38400 Saint-Martin d'Hères (France).

Key words
Water vapor; carbon dioxide; continuum absorption; CRDS; OFCEAS; planetary atmosphere

Abstract

Absorption spectra of humidified CO_2 have been recorded at room temperature by cavity enhanced absorption techniques (CRDS and OFCEAS): (i) in three spectral ranges of the 1.6 µm window (5720-6045 cm^{-1}; 6390-6460 cm^{-1} and 6570-6665 cm^{-1}), (ii) in four narrow spectral intervals of the 2.3 µm window (4243-4255 cm^{-1}; 4301.3-4302 cm^{-1}; 4421.5-4440 cm^{-1} and 4518-4535 cm^{-1}), and (iii) around 2853 cm^{-1}. All these spectral ranges are situated in transparency windows of both H_2O and CO_2. The binary absorption coefficients $(B_{CO_2-H_2O} + B_{H_2O-CO_2})$ are retrieved from low pressure spectra (<1atm) recorded with different molar fractions of water vapor in CO_2 after subtracting the H_2O and CO_2 local monomer contributions and the self-continuum contribution of each species (i.e. H_2O-H_2O and CO_2-CO_2). Experimental room temperature binary coefficients are then compared to the only available model based on line shape profiles with χ-factors. This model well reproduces our experimental values on the low- and high-frequency edges of the 1.6 µm window and gives a relatively good agreement for the 2853 cm^{-1} data point. Larger differences are observed in the 2.3 µm window where the calculated values are underestimated by a factor of 3. Around 6000 cm^{-1}, an additional absorption peak is observed which is tentatively interpreted as a collision induced absorption band of the H_2O and CO_2 molecules.

Introduction

The knowledge of the absorption of a gas mixture of water and CO_2 is required to better model the atmospheres of rocky planets with stronger constraints on the radiation budget. In addition to the contribution of the H_2O and CO_2 rovibrational lines which are proportional to their respective partial pressures, the mixture absorption includes binary contributions varying smoothly with the frequency: *(i)* the self-H_2O and self-CO_2 continua, with quadratic partial pressure dependence and *(ii)* the H_2O+CO_2 continuum which is the sum of two contributions, proportional to the product of the partial pressures: one due to H_2O molecules as absorbing molecules interacting with CO_2 colliding molecules and the other one due to CO_2 absorbing molecules interacting with H_2O colliding molecules.

During the early stage of their life, telluric planets, that have a liquid mantle, are supposed to outgas large quantities of volatiles mainly made up of H_2O and CO_2 [1,2,3,4]. A modeling, including accurate continua absorption, will give key insights on the rocky planets' evolution from this early stage and will help to understand, for example, why the evolution of Venus and Earth has been so different. It is also a key element in the modeling of the extra-solar planets' atmosphere where CO_2 dominates (Refs) leading to the generation of better observables for future observations, such as the innermost planets of the TRAPPIST-1 system with the forthcoming James Webb Space Telescope.

The accurate determination of the H_2O+CO_2 continuum is also of first importance to test the proposition according to which the formation of the Martian valley networks could be due to episodic precipitations trigged by meteoritic impacts injecting large quantities of H_2O and CO_2 in the planet's atmosphere [see for example 5,6].

Pioneer theoretical calculations of the far wing line shapes were performed by Ma and Tipping [7] based on a quasi-static and binary collision approach providing the H_2O continuum in CO_2 at 296 K in the 0-10 000 cm^{-1} spectral range. About 25 years later, the first experimental measurements of the H_2O+CO_2 continuum were reported in [8] for the 1100-1350 and 2450-2750 cm^{-1} spectral ranges at four temperatures (between 294 K and 339 K) with a Fourier transform spectrometer (FTS). This work showed that *(i)* near 1100 cm^{-1}, the measured H_2O continuum in CO_2 is about twenty times larger than in N_2, *(ii)* in the high frequency wing of the ν_3 band of CO_2 (around 2500 cm^{-1}), the continuum of CO_2 with H_2O as collision partner is an order of magnitude larger than the CO_2 self-continuum. These experimental data have been confirmed recently, by FTS at temperatures up to 367 K in the 2400-2600 cm^{-1} [9] and 100-1500 cm^{-1} [10] intervals. The latter reference validated the theoretical results of [7] in the considered range. In addition, an empirical modeling using a sub-Lorentzian line-shape with temperature-dependent correction factors χ was proposed to better reproduce the experimental data [9]. Recently, classical molecular dynamic simulations were carried out allowing

generation of the absorption spectrum of the H_2O broadened CO_2 spectrum in the high frequency wing of the ν_3 band [11]. Good agreement with the measurements of Refs. [9,10] was achieved without any adjusted parameters.

The aim of the present contribution is to provide additional experimental data points in different CO_2 and H_2O transparency windows (see **Figure 1**). These windows play a major role in radiative transfer as spectral regions corresponding to strong H_2O and CO_2 absorption bands are generally saturated. Due to the expected weak absorptions, highly sensitive spectroscopic techniques, namely cavity ring-down spectroscopy (CRDS) and optical feedback cavity enhanced absorption spectroscopy (OFCEAS) have been used to record spectra of CO_2+H_2O mixtures. The experimental setups are described in the next section (Section 2). The procedures adopted to record spectra and retrieve the binary coefficients are detailed in Section 3 as well as the error budget. Comparison between these experimental binary coefficients and the available models is presented and discussed in Section 4 before concluding remarks (Section 5).

1. Experimental setups

The CRDS and OFCEAS techniques have proven their ability to measure weak absorption continua for pure H_2O (see for example [12,13,14]), O_2 [15,16], CO_2 [17,18,19] and H_2O in air [20] gas samples. In this work, we applied our CRDS and OFCEAS spectrometers to the determination of the H_2O+CO_2 continuum in the 3.5 µm, 2.3 µm and 1.6 µm transparency windows. The spectral ranges together with the technique used and corresponding laser sources and experimental conditions are summarized in **Table 1**. All the studied spectral regions are located in transparency windows where both CO_2 and H_2O weakly absorb (**Figure 1**).

Spectral Range (cm^{-1})	Technique	Laser source	P_{tot} (Torr)	X_{H2O} (ppm)	T (K)
2852.7-2853.4	OFCEAS	ICL	450	5000 to 15000	303
4243-4255	CRDS	DFB LD	500	3000 to 10000	298
4301.3-4302	OFCEAS	DFB LD	700	5000 to 15000	306
4421.5-4440	CRDS	DFB LD	700	5000 to 15000	298
4518-4535	CRDS	DFB LD	500/700	5000 to 15000	298
5720-6045	CRDS	DFB LD	750	5000 to 15000	296
6390-6460	CRDS	DFB LD	750	10000	297.5
6570-6665	CRDS	DFB LD	750	3000 to 7000	298

Table 1. *Summary of the experimental conditions of the different recordings.* DFB LD *and* ICL *mean* distributed feedback laser diode *and* interband cascade laser*, respectively.*

1.1. The CRDS setup

The CRDS setups use as light sources a set of distributed feedback (DFB) laser diodes, from NTT Electronics Corporation and Eblana Photonics, allowing covering the entire 1.6 µm window (the gaps between the spectral ranges reported in **Table 1** for this window (see also **Fig. 1**) being due to the too strong absorption of CO_2) and three additional spectral intervals centred near 4250, 4430 and 4525 cm^{-1} (from Nanoplus GmbH). These latter sources are narrowed by an optical feedback scheme adapted from [21] to increase the injection efficiency into the high finesse cavity and improve the absorption sensitivity. Note that each laser diode can be tuned over a few tens cm^{-1}. The cavity ring down spectrometers use 142 cm long high finesse cavities fitted with different sets of highly reflective dielectric mirrors optimized for the 4000-4550, 4550-5130, 5300-6000 and 5700-6670 cm^{-1} spectral ranges depending of the laser diode used. To achieve resonances between the laser emission and a longitudinal mode of the optical cavity, the output mirror of the cavity is placed on a PZT tube supplied by a triangular voltage allowing for dithering the cavity length and periodically obtaining build-up events. For build-up event with a photodiode signal higher than a user-defined threshold, $I_{threshold}$, an acousto-optic modulator switched off the laser light leading to a purely exponential decay signal on the photodiode corresponding to a ring down (RD) event expressed by:

$$I(t) = I_{threshold} \exp(-t/\tau) \quad (1)$$

where τ is the ring-down (RD) time.

The absorption coefficient at the laser frequency, ν, is then derived from the following equation:

$$\alpha(\nu) = \frac{n}{c\,\tau(\nu)} - \frac{n_{Ar}}{c\,\tau_0(\nu)} \quad (2)$$

where c is the speed of light, τ_0 the ring down time for the cell filled with argon (which is a non absorbing gas used here to determine the baseline absorption $n_{Ar}/c\tau_0$) and n and n_{Ar}, the refractive index of the absorbing gas and of argon, respectively.

The absorption spectra are recorded by tuning step-by-step the laser diode temperature and thus the emitted frequency, keeping unchanged the injection current. Typically, ten RD times are averaged at each spectral step. A part of the laser light is also sent into a wavelength meter (model 621-A IR from Bristol) to monitor the laser frequency. The intra-cavity pressure is monitored by a pressure sensor from Edwards (1000 mbar full scale, accuracy 0.15 % of reading). The cavity temperature is not stabilized and is close to room temperature (see **Table 1**).

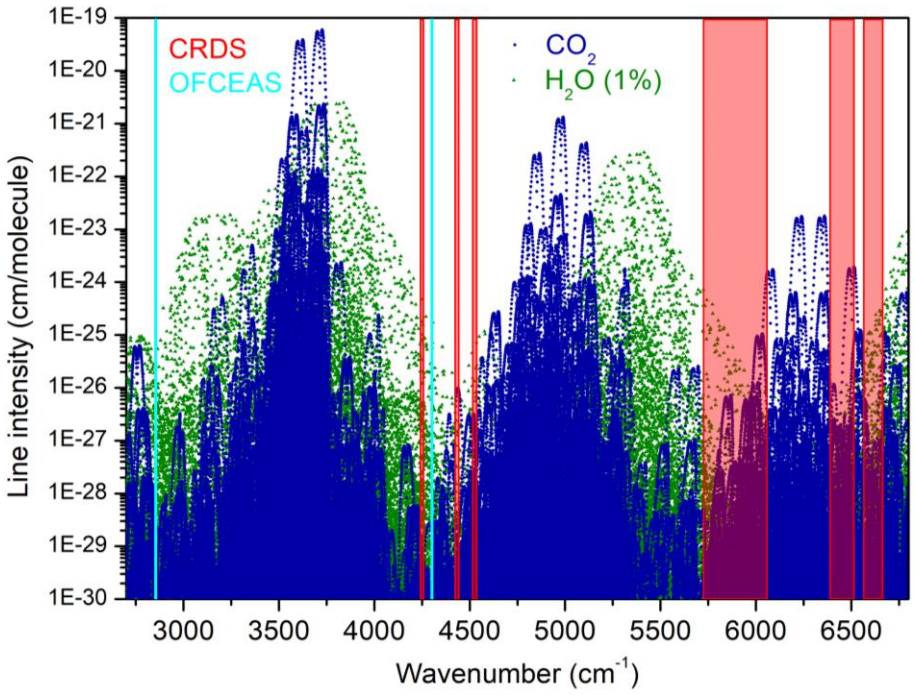

Figure 1. *Overview of the H_2O and CO_2 absorption lines provided by the HITRAN2016 database [22] between 2700 cm^{-1} and 6800 cm^{-1}. The vertical light blue solid lines and red rectangles indicate where measurements were performed using OFCEAS and CRDS, respectively. The line intensities of water vapor have been divided by a factor 100 to roughly scale to the relative contributions of H_2O and CO_2 in the used gas mixtures.*

2.2 OFCEAS setup

The application of the OFCEAS technique to continua measurements has been described in detail in [14]. Basically, this high-sensitivity technique exploits optical feedback, from a V-shape high-finesse cavity, towards the diode laser source. This feedback appears at cavity resonances and leads to laser emission width narrowing and to a temporary frequency locking to the cavity mode which ensures an optimized cavity injection by the laser radiation. The laser frequency is scanned with fast laser current ramps (at a typical frequency of 5 Hz). During these ramps, the laser is successively locked to the different cavity modes leading to transmission spectra after dividing the cavity output signal by the reference laser power signal at each cavity-mode maximum. The transmission spectra are then converted into cavity-loss spectra with an absolute absorption scale after calibration with a ring-down measurement [23]. In this technique, the spectrum data points are equally spaced by the cavity free spectral range. Note that the phase and the coupling rate of the optical feedback are controlled respectively to improve the injection of the cavity modes and increase the time during which the laser remains locked.

In this work, two OFCEAS setups have been used. The first one is based on an interband cascade laser (ICL) source centred at 2853 cm^{-1} from Nanoplus GmbH and high reflectivity mirrors from Layertec GmbH providing a reflectivity of 99.99 % at this wavenumber. Ring-down times of 13 µs are measured for an unfolded V-shaped cavity length of 80 cm. Variations of the baseline of 5×10^{-9} cm^{-1}

are observed for that setup requiring averaging typically 100 spectra to determine the mean baseline. In the second setup, a DFB laser diode (from Nanoplus GmbH) emitting near 4302 cm^{-1} and a set of three high reflectivity mirrors with a reflectivity of 99.997 % at this wavenumber were used, all the rest being identical to the first setup. This latter setup allows reaching RD times of 45 µs, and a baseline stability of 2×10^{-9} cm^{-1}. An averaging over 100 spectra was also used. Spectral point spacing was equal to the free spectral range of the cavity (*FSR* = 187.5 MHz) while the absolute frequency calibration relied on comparing fitted values of line centres to reference line positions [22].

In both cases, it is possible to stabilize the cell within the temperature range 303-323 K with ±0.3 K accuracy by using platinum thermistances and a heating ribbon. The intra-cavity pressure is monitored by a pressure sensor (STS ATM1ST, 1 bar full scale, accuracy 0.1 % of full scale).

2.3 Humidity generator and determination of the water vapor partial pressure

For all the CRDS and OFCEAS measurements, series of spectra are recorded for H_2O+CO_2 mixtures with different molar fractions of H_2O (between 3000 and 15000 ppmv) and total pressures (between 300 and 750 Torr) (see **Table 1**). For that, a gas flow of H_2O+CO_2 is produced thanks to a commercial humidity generator (from Omicron Technologies) based on a temperature regulated membrane system to generate pure water vapor. Water vapor is then mixed with the dry carrier gas (here CO_2) with a proportional control solenoid valve with bypass to achieve the desired humidity level. The gas flow (300 sccm) as well as the pressure (1045 mbar) are regulated in the exit line by a mass flow controller (Area model, FC-R7800 series from Hitachi Metals Ltd.) and a back pressure controller (Model IQP-700C from Bronkhorst). Only a limited part of this flow (typically a few tens sccm) is derived into the CRDS or OFCEAS high finesse cavity to avoid dirtying the mirrors by displacing small particles inevitably present on the walls of the cavity. The pressure in the CRDS cavity is maintained at a fixed value with a solenoid valve and a proportional integral software based loop acting on the gas flow. In the OFCEAS setups, the gas flow and intra-cavity pressure were regulated using Bronkhorst modules. In addition, the remote head of a precision chilled mirror hygrometer (Model S8000 from Mitchell) is placed on the exit line to provide a direct measurement of the dew or frost point temperature. After calibration at CETIAT [24], the dew point temperature is known with a 2σ-uncertainty better than 0.1°C over the -20°C to +20°C range. A PID loop acting on the solenoid valve with bypass of the humidity generator is used to maintain the dew point at the chosen set point. This system is able to produce a flow of CO_2 where the H_2O molar fraction varies by no more than 0.1% (peak to peak) during several hours for set points in the 5000 - 15000 ppmv range.

To retrieve the molar fraction, the dew point temperature is first converted into saturated vapor pressure (corresponding to the water vapor partial pressure, P_{H2O}) using formulas given by [25,26] for liquid water and ice. The partial pressure values are then multiplied by an enhancement factor

(calculated from [27,28]) to take into account non-ideal gas effects and the small departures from ideal solution behaviour with regard to equilibrium between the gas mixture and condensed phase located at the sensing surface of the chilled-mirror hygrometer. For our pressure and temperature conditions, this factor is lower than 1.004. Knowing the total pressure, P_{tot_EL}, in the exit line (EL) (measured by a Wika pressure gauge; 1.6 bar full scale; 0.1% accuracy), we deduce the molar fraction of water vapour $X_{H2O}= P_{H2O\_EL}/P_{tot\_EL}$. After having flushed during several hours the high finesse cavities with a flow of CO_2 with constant water vapor molar fraction, we make the hypothesis that this latter quantity is the same in the high finesse cells than in the exit line, so that we can also derive the water vapor partial pressure in the cell as $P_{H2O} = X_{H2O}P_{tot}$ where P_{tot} is the intra-cavity pressure. Densities of CO_2, ρ_{CO2}, and H_2O, ρ_{H2O}, are then calculated knowing the cell temperature measured with a Pt 100 sensor calibrated at CETIAT (2σ-uncertainty ±0.06°C) fixed on the external wall of the cavity underneath the enveloping thermal insulation foam.

P_{H2O} can also be retrieved from a fit of a selection of water vapor lines with intensity provided with a high accuracy (1 to 2%) in the HITRAN database. Comparison between those two methods shows that differences can occur. More precisely, in the CRDS setup used for measurements between 5730 and 5950 cm^{-1}, we obtained lower P_{H2O} values than expected from the chilled-mirror hygrometer due to adsorption on the gas line going to the CRDS cell for all molar fractions considered in this study, with an average relative difference ranging from 2% for a molar fraction of 5000 ppm, to 6% at 15000 ppm. However, at a lower molar fraction of 1000 ppm (not used for continua measurements), P_{H2O} values derived from the fit were larger than expected, due to outgasing. For all the scans recorded with this setup, the P_{H2O} value derived from the fitted line absorption has been adopted. This effect has been minimized for the measurements between 5950 and 6660 cm^{-1} by replacing the tubes in the gas line with tubes having a Sulfinet surface treatment (from Restek company) limiting water adsorption.

In the case of the OFCEAS measurements near 2 µm and 3.5 µm, this effect was considered to be below the 2 % uncertainty on water molar fraction and the P_{H2O} value derived from the hygrometer dew point temperature was adopted. For the CRDS measurements in the 2.3 µm window, the value of P_{H2O} was determined from fitted line absorption.

2. Recordings and retrieval of the binary coefficients

3.1 CRDS spectra

In the 2.3 µm window, spectra were acquired in the following manner. For each total pressure and molar fraction conditions, a sequence of one argon spectrum, two H_2O+CO_2 spectra and a second argon spectrum was recorded, emptying the cavity before each change of the gas composition. Such a sequence (**Figure 2**) allows *(i)* checking the water vapour stability in the mixture, *(ii)* accurately determining the spectrum baseline, as argon does not absorb, and *(iii)* checking the

baseline stability after pumping and filling cycles. Baseline stability of the order of 10^{-10} cm^{-1} was achieved for the CRDS spectra near 4525 cm^{-1} while a stability of a few 10^{-9} cm^{-1} was observed near 4250 cm^{-1} and 4430 cm^{-1}. This larger value results from the fact that the coating of one of the mirrors was damaged, making the baseline more sensitive to changes in the mirrors alignment.

In the 1.6 µm window, the cavity alignment was more sensitive to large pressure variations. Hence, the intra-cavity pressure was kept constant throughout an entire measurement, while argon and H_2O+CO_2 mixtures were alternatively flowed through the cavity. In this case the observed baseline stability was on the order of a few 10^{-10} cm^{-1}.

Measurements were repeated for several values of water molar fraction in each spectral region (see **Table 1**) to ensure the linearity of the obtained binary absorption coefficient with respect to the density product.

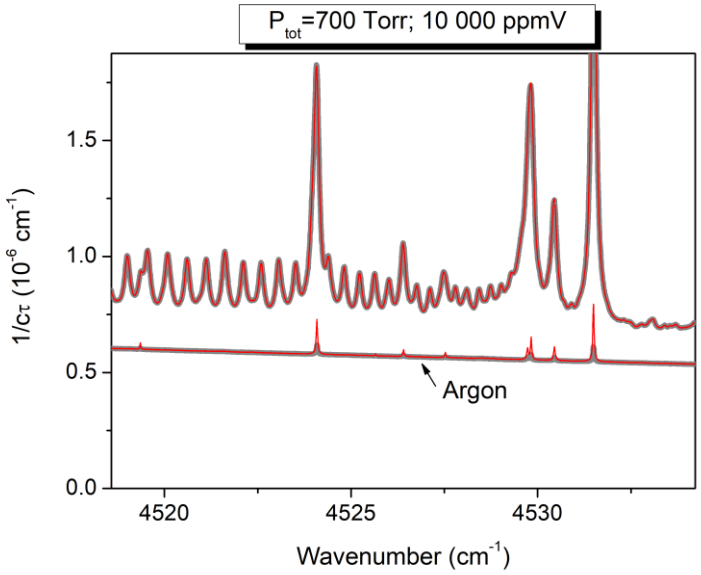

Figure 2. *Spectra of argon and of a (H_2O+CO_2) mixture recorded at a total pressure of 700 Torr recorded by CRDS near 4525 cm^{-1}. The water vapor molar fraction in the mixture was 10 000 ppmv. The argon spectra (lower ones) recorded at the beginning (I) and at the end (4) of the 4 step-procedure give the zero-absorption baseline which is subtracted from the (H_2O+CO_2) spectra (2) and (3). At the scale of the figure, the spectra (2) and (3), recorded successively are indistinguishable illustrating the stability of the setup. Note the water vapor traces (at the 100 ppm level) are present in the argon spectra.*

3.2 OFCEAS spectra

For OFCEAS spectra, the recording sequence was as follows. In a first step, dry nitrogen was flowed through the cavity to measure the baseline losses. As spectra were recorded continuously, monitoring the absorption after the gas source was switched to the H_2O+CO_2 mixture allowed to check the stability of the gas inside the cavity. Once the absorption had become stable, 100 spectra were averaged before modifying the water molar fraction set point on the hygrometer. In total, four values of the water molar fraction were used: 5 000, 10 000, 12 500 and 15 000 ppmv (see **Table 1**).

3.3 Retrieval of the H_2O+CO_2 binary coefficients

For each series of spectra, the zero-absorption baseline was determined by fitting the argon or nitrogen spectrum with a second order polynomial, after removing the water lines (in traces). The baselines were then subtracted from the H_2O+CO_2 spectra. In the 1.6 µm window, the Rayleigh scattering losses due to CO_2 differ from those due to argon by a few 10^{-9} cm^{-1} [29,30] and the corresponding difference was taken into account. In the other spectral windows, Rayleigh losses are much smaller and negligible. As a result, the absorption coefficient, $\alpha(\nu)$, can be expressed as:

$$\alpha(\nu,T) = M_{CO_2}\rho_{CO_2} + M_{H_2O}\rho_{H_2O} + B_{CO_2-CO_2}\rho_{CO_2}^2 + B_{H_2O-H_2O}\rho_{H_2O}^2 + (B_{CO_2-H_2O} + B_{H_2O-CO_2})\rho_{CO_2}\rho_{H_2O} \quad (3)$$

where $M_{CO_2}\rho_{CO_2}$ and $M_{H_2O}\rho_{H_2O}$ are the contributions due to the "monomer local lines" of CO_2 and H_2O, respectively and ρ represents the density. The B_{i-j} coefficients (in $cm^{-1}amagat^{-2}$) correspond to the binary coefficients, where *i* denotes the absorbing gas and *j* the perturber.

The $(B_{CO_2-H_2O} + B_{H_2O-CO_2})$ binary coefficient (the two contributions are indistinguishable experimentally) is obtained from $\alpha(\nu)$, after subtraction of the other terms appearing in Eq. (3). First, we used the HITRAN2016 database [22] to simulate the local CO_2 and H_2O monomer contributions with Voigt profiles truncated at ±25 cm^{-1} excluding the pedestal of the absorption lines [31]. As CO_2-broadening coefficients for H_2O are not given in HITRAN, the air-broadening coefficients were multiplied by a factor of 1.67 following the value reported in [32] for the water vapor rotational band spectral region, and fitted for the most intense lines. Note that for the spectra around 2853 cm^{-1}, the H_2O local monomer absorption is mainly due to HDO for which we take an isotopic abundance 20 % lower than the one given in HITRAN2016 as determined in our previous water samples (see for instance [33]). The CO_2 cylinder used for this study contained methane impurities. In the 2853 cm^{-1} spectra, two CH_4 lines of intensity greater than 10^{-22} cm/molecule allowed determining a CH_4 molar fraction of about 590 ppb. The methane lines were included in the monomer resonance line simulations for all spectra, although their contribution is mostly negligible except near 2853 cm^{-1}.

Table 2 summarizes the source of the water and CO_2 self-continuum cross sections used to subtract their corresponding contributions from the recorded spectra.

Spectral range (cm^{-1})	Water self-continuum	CO_2 self-continuum
2853	Fleurbaey in press [35]	This work
4244-4256	Mondelain 2015 [34]	Tonkov 1996 [37]
4302	Ventrillard 2015 [14]	Tonkov 1996 [37]
4421-4440	Richard 2017 [13]	Tonkov 1996 [37]
4518-4535	Campargue 2016 [33]	Tonkov 1996 [37]

5730-5800	Vasilchenko 2019 [20]	Mondelain 2017 [19]
5800-6665	Vasilchenko 2019 [20]	This work

Table 2. *Summary of the sources of the self-continuum coefficients used in this work. Note that near 2853 cm^{-1}, the CO_2 self-continuum and local line absorption were subtracted together from the mixture spectra, so that the value of the self-continuum was not derived in this work.*

The water vapor self-continuum contributions were obtained from the cross-sections reported in our previous papers [13,14,20,34,35], except at 2853 cm^{-1} where this value was newly determined and found to be 5.85(42)×10^{-24} cm^2 molec^{-1} atm^{-1} [36].

In the case of the CO_2 self-continuum, the $B_{CO_2-CO_2}\rho_{CO_2}^2$ contributions were calculated from the measurements of [37] in the 2.2 µm window, and of [19] in the 1.6 µm window below 5800 cm^{-1}. In all other spectral regions, the CO_2 self-continuum cross-sections values were obtained from dedicated measurements as follows. The high finesse cell was filled with pure CO_2 gas at a pressure value equal to the total pressure used in the binary absorption experiments. The contribution from the monomer lines was subtracted as described above, and the remaining absorption was divided by $\rho_{CO_2}^2$ to retrieve the self-continuum coefficient $B_{CO_2-CO_2}$. The obtained values were smoothed using polynomial fits as a function of wavenumber, in order to calculate the self-continuum contribution to the H_2O-CO_2 measurements. For the spectral point at 2853 cm^{-1}, the total absorption due to CO_2 (local lines and self-continuum) was retrieved from these pure CO_2 spectra and subtracted from the water+CO_2 mixture spectra recorded for the same CO_2 partial pressure, so that the self-continuum coefficient $B_{CO_2-CO_2}$ was not itself determined.

Smoothed values of the self-continuum absorption coefficients of water vapor and carbon dioxide used in this work are provided in a *Supplementary Material* together with their estimated uncertainty and their source. **Figure 3** displays the different contributions to the absorption coefficient recorded around 4525 cm^{-1} for a total pressure of 700 Torr and a water vapor molar fraction of 10 000 ppm. In these conditions, the local line contribution of CO_2, due to the 00021-00001 band of the $^{16}O^{13}C^{18}O$ isotopologue in natural abundance, dominates. In other spectral regions like near 4250 cm^{-1}, the local line contribution of water vapor is the largest subtracted absorption.

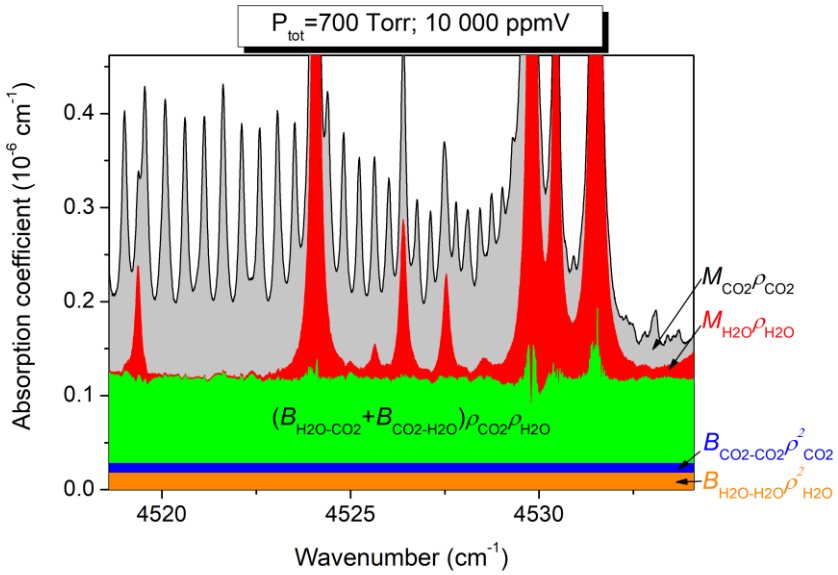

Figure 3. *The different contributions to the total absorption coefficient measured by CRDS around 4525 cm^{-1} for a mixture of 10 000 ppmv of H_2O in CO_2 at a total pressure of 700 Torr. Refer to the text for the different notations.*

At all the wavenumbers studied here, the absorption coefficient reduced by the two self-continua contributions and the resonance line contribution is found to be proportional to $\rho_{CO_2}\rho_{H_2O}$, as illustrated in **Figure 4** (lower panel). This leads to a very good consistency of the binary coefficients retrieved for the different densities of CO_2 and H_2O in the 2.3 µm window (**Figure 4**, upper panel), as well as in the other spectral regions, as shown in **Figure 5** for the 1.6 µm window.

The retrieved binary coefficients are given in the Supplementary material along with their type-B uncertainty (see next section). We also provide smoothed values of the binary coefficient for ease of use, with a combined (type-A and type-B) uncertainty. These smoothed values are used in **Figure 6** along with other calculated contributions to the absorption, to illustrate the various contributions to the absorption in part of the 1.6 µm window.

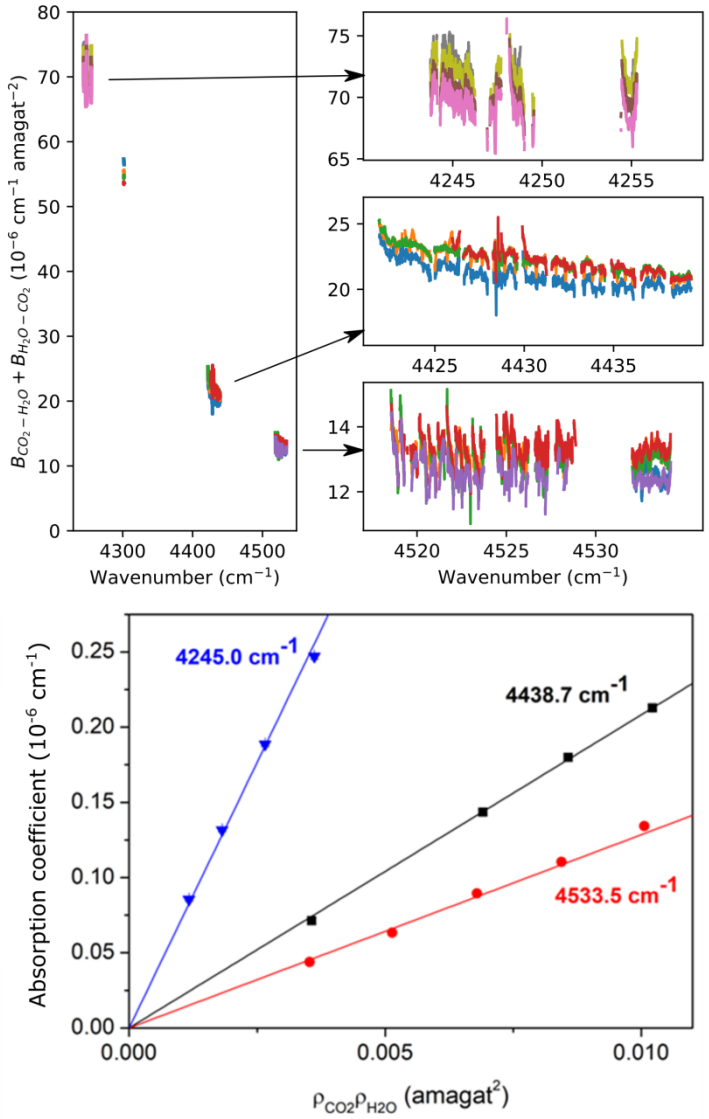

319

320 ***Figure 4.*** *Absorption coefficients due to the* $(\boldsymbol{B_{CO_2-H_2O}} + \boldsymbol{B_{H_2O-CO_2}})\boldsymbol{\rho_{CO_2}\rho_{H_2O}}$ *contribution (lower panel) and*
321 *retrieved binary coefficients versus wavenumber (upper panel) for different water vapor and* CO_2 *densities*
322 *(corresponding to different colors).*

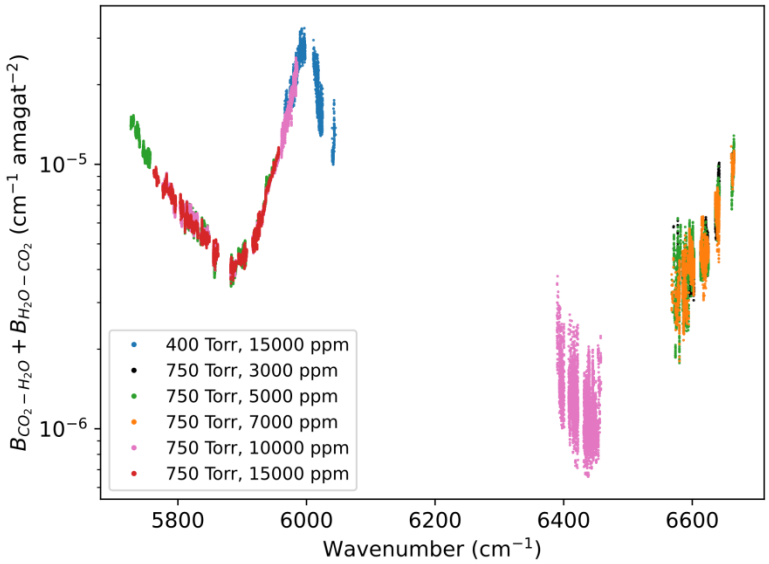

Figure 5. *Overview of the binary coefficients measured in the 1.6 µm window for various total pressures and water vapor molar fractions.*

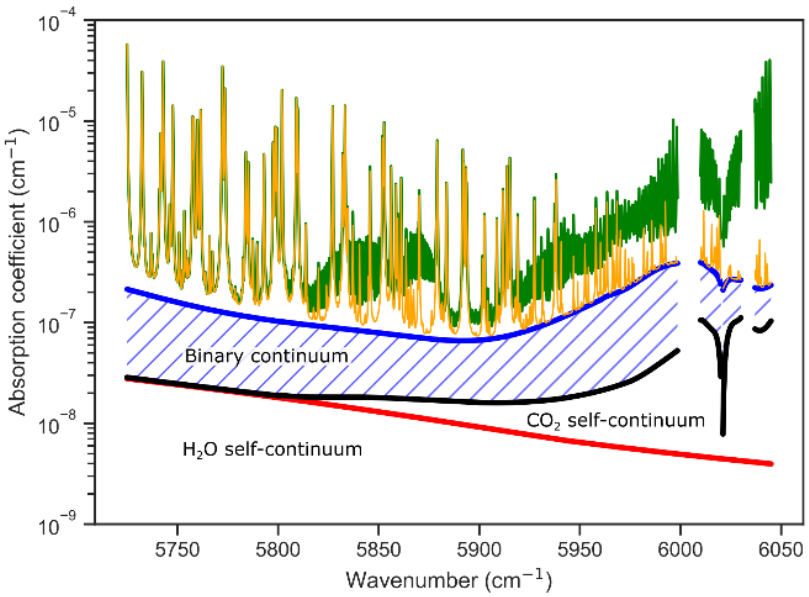

Figure 6. *Overview of the various contributions to absorption in the low-frequency part of the 1.6 µm window, for a pressure of 700 Torr and a water mole fraction of 15 000 ppm. The self-continua contributions (water, red and CO_2, black) are calculated using the coefficients listed in the Supplementary Material (see sources in Table 2). The (H_2O+CO_2) binary continuum (hatched blue) corresponds to the smoothed values reported in the Supplementary Material. The water (yellow) and CO_2 (green) local line contributions are HITRAN simulations, with collisional broadening multiplied by 1.67 for CO_2-broadened water.*

3.4 Estimated uncertainties on the experimental binary coefficients

The uncertainties on the derived ($B_{CO_2-H_2O} + B_{H_2O-CO_2}$) binary coefficients have been calculated with the error propagation approach using Eq. (1), assuming uncorrelated variables. Uncertainty on

total pressure and temperature are estimated to 0.15% and 0.1K, respectively. A baseline uncertainty of 5×10^{-10} cm^{-1} is adopted for the 1.6 µm window and for the measurements centered at 4525 cm^{-1}. At 2853, 4250, 4302 and 4430 cm^{-1}, the baseline uncertainties are taken as equal to 5×10^{-9}, 2×10^{-9}, 1×10^{-8} and 2×10^{-9} cm^{-1}, respectively. Baseline stability was estimated from argon or nitrogen spectra.

As mentioned above, uncertainties on water vapor and carbon dioxide binary coefficients are reported as *Supplementary Materials*. The uncertainty on the water vapor partial pressure is the main contributor to the final error budget due to the local monomer contribution and to the self-continuum contribution (see Figs. 4 and 6). As explained in part 2.3, the water vapor partial pressures retrieved from the dew/frost point temperature measured with the chilled-mirror hygrometer are in some cases slightly different from the ones derived from the recorded spectra. These latter are adopted to extract the binary coefficients ($B_{CO_2-H_2O} + B_{H_2O-CO_2}$) from the spectra recorded between 5730 and 5950 cm^{-1} and the CRDS measurements in the 2.3 µm window, the values from the hygrometer being used in all other cases. A mean uncertainty of 2% is estimated for P_{H2O}. In the case of P_{CO2}, the estimated uncertainties are much smaller and correspond to the uncertainty on the total pressure (0.15%).

The H_2O and CO_2 local monomer contribution uncertainties are determined by taking into account the error bars on the line intensities, self-broadening, air-broadening coefficients and partial pressures. The uncertainties on the line parameters were taken from the HITRAN database [22]. In both cases (*i.e.* for H_2O and CO_2), four simulations are performed, each of them with either, the intensities, γ_{self} , γ_{air} coefficients or P_i values increased by their error bar. The resulting deviations from the HITRAN simulation, $\delta_i(\nu)$, lead to the uncertainty on α_{WML}: $\delta\alpha_{WML}(\nu) = \left[\sum_{i=1}^{4} \delta_i^2(\nu)\right]^{1/2}$.

The uncertainties detailed above are of type-B. Statistical (type-A) uncertainties are taken as the standard deviation of the experimental data fit residuals. Final residuals given in Supplementary material correspond to the sum in quadrature of type A and B uncertainties.

4 Semi-empirical calculations and comparison with available experimental data

Few measurements of H_2O+CO_2 continua are available in the literature [8,9,10], all by FTS. **Table 2** summarizes the main experimental characteristics showing that only the work of [8] provides data to compare with. More precisely, in this latter study, a value of $4(\pm1)\times10^{-5}$ cm^{-1}amagat^{-2} was reported around 2850 cm^{-1} for the $B_{CO_2-H_2O} + B_{H_2O-CO_2}$ binary coefficient with no observed temperature dependence. This value is 1.5 times higher than what we measured here ($2.66(\pm0.32)\times10^{-5}$ cm^{-1} amagat^{-2}). These two measurements are thus barely compatible considering their *1σ*-error bars.

Ref.	Absorber	Collider	Spectral range (cm^{-1})	Temp. (K)
[8]	H_2O	CO_2	1080-1330	296-340

	CO_2	H_2O	2500-3300	296-340
[9]	CO_2	H_2O	2400-2600	325-367
[10]	H_2O	CO_2	100-1500	296, 325,366

Table 2. *Summary of the experimental works on H_2O+CO_2 continuum available in the literature.*

From a theoretical point of view, recent progress has been done for the calculations of the far wings and collision induced absorption (CIA) with the classical molecular dynamic simulations (CMDS) which provide, as explained in [38], "the center-of-mass positions and orientations of many (rigid) linear molecules interacting through an input anisotropic potential". The auto-correlation functions (ACF) of the allowed- and induced-dipoles and of their cross-terms are then computed. The absorption spectrum is finally obtained after applying a Fourier-Laplace transform to these ACF. This approach has been applied to systems like CO_2–CO_2 in [39,40], CO_2–H_2O and N_2–H_2O in [38] where the first molecule is the absorbing molecule and the second one the collider. Good agreements with measured data have been obtained, without any scaling factor, for the ν_3 band for pure CO_2, the high frequency wing of this band for CO_2 in H_2O and the CIA of the N_2 fundamental band. Up to now, CMDS has only been applied to linear absorbing molecules and thus not to the water molecule as absorber so that the $B_{H_2O-CO_2}$ coefficient has not yet been calculated.

Another way to get (independently) the $B_{H_2O-CO_2}$ and $B_{CO_2-H_2O}$ coefficients consists in adopting the widespread χ-factor empirical approach. Here, the Lorentzian/Voigt line-shape is corrected by applying χ-factors in the wings of the profile depending on the distance to the line center. The same profile is applied to all the transitions of the absorbing molecule which are provided by a spectroscopic database such as HITRAN. For the H_2O absorbing molecule in CO_2, the χ-factors have been obtained either by using quasi-static predictions [7] or by fitting these factors on experimental data sets as done in [10] with FTS data in the 100-1500 cm^{-1} spectral range. The same procedure was applied to CO_2 as absorbing molecule and H_2O as collider in the 2400-2600 cm^{-1} spectral range [9].

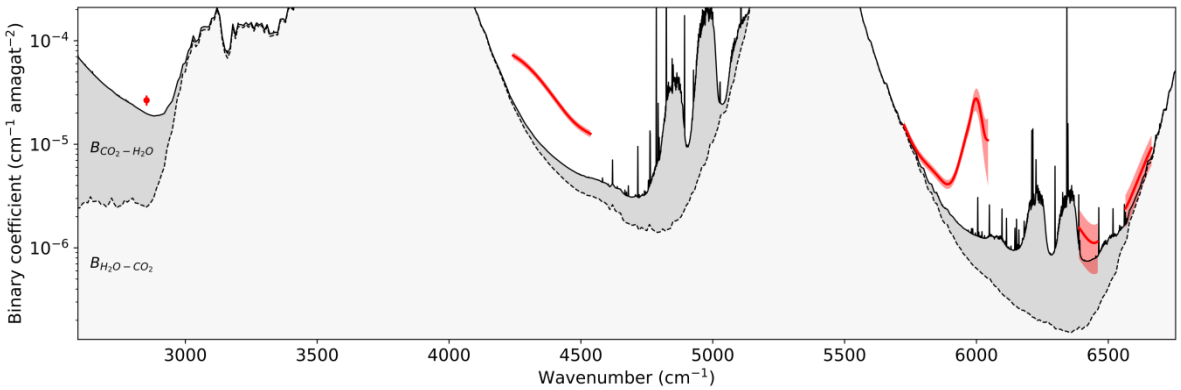

Figure 7. *Overview of the experimental and calculated binary coefficients obtained for H_2O+CO_2 mixture. The calculated coefficients are obtained with the χ-factor approach adopted in [10] for $B_{CO2\text{-}H2O}$ and [10] for $B_{H2O\text{-}CO2}$. The black solid line corresponds to the sum of these two calculated binary coefficients, while the dashed line presents $B_{H2O\text{-}CO2}$. The smoothed experimental values are plotted as a red solid line with a shaded area corresponding to the 1σ uncertainty.*

Figure 7 shows the different data sets mentioned just above as well as the sum of the binary coefficients calculated in the present work using the χ-factor approach developed in [9,10] and the data obtained in this work. As can be seen, the χ-factor approach well reproduces our experimental binary coefficients on the low- and high-frequency edges of the 1.6 µm window and a relatively good agreement is observed for the 2853 cm^{-1} data point. Larger differences are observed in the 2.3 µm window where the calculated values underestimate by factors between 2.6 and 3.9 our experimental data. This is not so surprising considering that the χ-factor approach has limited extrapolation capabilities [41]. Interestingly, unexpected peak absorption is observed around 6000 cm^{-1} that we interpret as a signature of the collision induced absorption (CIA) corresponding to the $\nu_3(CO_2)$ + $\nu_1(H_2O)$ simultaneous transition. Note that the possible detection of this combination band was anticipated in Ref. [42]. Further investigations dedicated to this absorption peak will be done in a future work. In all cases, this additional absorption is not taken into account in the χ-factor approach.

5 Conclusion

From spectra of water vapor in CO_2 mixtures recorded with highly sensitive and stable CRDS and OFCEAS techniques, we derived the binary coefficients $B_{CO_2-H_2O} + B_{H_2O-CO_2}$ at room temperature in different spectral regions corresponding both to H_2O and CO_2 spectral windows. To our knowledge, this constitutes the first experimental dataset of the H_2O+CO_2 continuum in those spectral regions. Comparison to values obtained from the only available model based on the χ-factor approach is presented. For that, binary coefficients are extrapolated in the spectral intervals studied in this work using a model where the χ-factors were previously fitted to FTS data recorded in the 100-1500 cm^{-1} spectral range for H_2O absorbing molecules in CO_2 [10] and in the 2400-2600 cm^{-1} spectral range [9] for the CO_2 absorbing molecules in H_2O. This comparison shows the ability of the model to quite well reproduce our experimental values on the edges of the 1.6 µm window and at 2853 cm^{-1} but a discrepancy is observed in the 2.3 µm window. It is important to notice that a peak of additional absorption (not predicted by the far-wing model) is observed around 6000 cm^{-1}. This peak is interpreted as due to a CIA band corresponding to a cooperative excitation of CO_2 and H_2O molecules. Additional work is planned to confirm this hypothesis and, if applicable, to model the collision induced absorption band of the H_2O and CO_2 molecules which has to be added to the far-wings contribution. The impact of this kind of CIA bands in other spectral regions remains to be evaluated. Finally, a study of the temperature dependence of the different contributions of the H_2O+CO_2 continuum is also of first importance for planetary applications and will be the subject of new dedicated measurements.

Acknowledgements

This work was performed in the frame of the ANR project *COMPLEAT* (ANR-19-CE31-0010-01). Authors want to thank J-M. Hartmann (LMD) for fruitful discussions and H. Tran (LMD) and M. Turbet (Univ. of Geneva) for providing them extended χ-factor data.

References

[1] Marcq E, Salvador A, Massol H, Davaille A. Thermal radiation of magma ocean planets using a 1-D radiative-convective model of H_2O-CO_2 atmospheres. J Geophys Res Planets 2017;122:1539–1553. Doi:10.1002/2016JE005224

[2] Abe Y, Matsui T. Evolution of an impact-generated H_2O-CO_2 atmosphere and formation of a hot proto-ocean on Earth. J Atmos Sci 1988;45:3081–3101. Doi:10.1175/1520-0469.

[3] Elkins-Tanton LT. Linked magma ocean solidification and atmospheric growth for Earth and Mars. Earth Planet Sci Lett 2008;271:181–191. Doi:10.1016/j.epsl.2008.03.062.

[4] Hamano K, Abe Y, Genda H. Emergence of two types of terrestrial planet on solidification of magma ocean. Nature 2013;497:607–610. Doi:10.1038/nature12163.

[5] Segura TL, McKay CP, Toon OB. An impact-induced, stable, runaway climate on Mars. Icarus 2012 ;220: 144–148. Doi:10.1016/j.icarus.2012.04.013

[6] Segura TL, Toon OB, Colaprete A. Modeling the environmental effects of moderate-sized impacts on Mars. J Geophys Res E Planets 2008;113:1–15. Doi:10. 1029/2008JE003147

[7] Ma Q, Tipping RH. A far wing line shape theory and its application to the foreign broadened water continuum absorption. III. J Chem Phys 1992;97:818-28.

[8] Baranov YI. On the significant enhancement of the continuum-collision induced absorption in H_2O+CO_2 mixtures. J Quant Spectrosc Radiat Transf 2016;175:100-6. doi:10.1016/j.jqsrt.2016.02.017

[9] Tran H, Turbet M, Chelin P, Landsheere X. Measurements and modeling of absorption by CO_2+H_2O mixtures in the spectral region beyond the CO_2 ν_3 -band head. Icarus 2018;306:116–121. Doi: 10.1016/j.icarus.2018.02.009

[10] Tran H, Turbet M, Hanoufa S, Landsheere X, Chelin P, Ma Q, Hartmann J-M. The CO_2–broadened H_2O continuum in the 100–1500 cm^{-1} region: Measurements, predictions and empirical model. J Quant Spectrosc Radiat Transf 2019;230:75-80. Doi: 10.1016/j.jqsrt.2019.03.016.

[11] Hartmann J-M, Boulet C, Tran DD, Tran H, Baranov Y. Effect of humidity on the absorption continua of CO2 and N2 near 4 µm: Calculations, comparisons with measurements, and consequences for atmospheric spectra. J Chem Phys 2018;148:054304. doi:10.1063/1.5019994

[12] Lechevallier L, Vasilchenko S, Grilli R, Mondelain D, Romanini D, Campargue A. The water vapour self-continuum absorption in the infrared atmospheric windows: new laser measurements near 3.3 and 2.0 µm. Atmos Meas Tech 2018;11:2159–2171. Doi: 10.5194/amt-11-2159-2018

[13] Richard L, Vasilchenko S, Mondelain D, Ventrillard I, Romanini D, Campargue A. Water vapor self-continuum absorption measurements in the 4.0 and 2.1 µm transparency windows. J Quant Spectrosc Radiat Transfer 2017;201:171–179. Doi: 10.1016/j.jqsrt.2017.06.037

[14] Ventrillard I, Romanini D, Mondelain D, Campargue A. Accurate measurements and temperature dependence of the water vapor self-continuum absorption in the 2.1 µm atmospheric window. J Chem Phys 2015;143:134304. Doi:10.1063/1.4931811.

[15] Mondelain D, Kassi S, Campargue A. Accurate laboratory measurement of the O_2 collision-induced absorption band near 1.27 µm. J Geophys Res: Atmosphere 2019;124:414–423. Doi :10.1029/2018JD029317

[16] Kassi S, Guessoum S, Abanto JCA, Tran H, Campargue A, Mondelain D. Temperature dependence of the collision-induced absorption band of O_2 near 1.27 µm. J Geophys Res: Atmospheres 2021;126:e2021JD034860. Doi :10.1029/2021JD034860

[17] Kassi S, Campargue A, Mondelain D, Tran H. High pressure Cavity Ring Down Spectroscopy: Application to the absorption continuum of CO_2 near 1.7µm. J Quant Spectrosc Radiat Transf 2015;167:97–104. Doi :10.1016/j.jqsrt.2015.08.014

[18] Mondelain D, Vasilchenko S, Čermák P, Kassi S, Campargue A. The CO_2 absorption spectrum in the 2.3 µm transparency window by high sensitivity CRDS: (II) Self-absorption continuum. J Quant Spectrosc Radiat Transfer 2017;187:38–43. Doi: 10.1016/j.jqsrt.2016.09.003
[19] Mondelain D, Campargue A, Čermák P, Gamache RR, Kassi S, Tashkun SA, Tran H. The CO_2 absorption continuum by high pressure CRDS in the 1.74 µm window. J Quant Spectrosc Radiat Transfer 2017;203:530–537. Doi: 10.1016/j.jqsrt.2017.02.019
[20] Vasilchenko S, Campargue A, Kassi S, Mondelain D. The water vapour self- and foreign-continua in the 1.6 µm and 2.3 µm windows by CRDS at room temperature. J Quant Spectrosc Radiat Transfer 2019;227:230–238. Doi: 10.1016/j.jqsrt.2019.02.016
[21] Lin Q, Van Camp MA, Zhang H, Jelenković B, Vuletić V. Long-external-cavity distributed Bragg reflector laser with sub kilo hertz intrinsic linewidth. Opt Lett 2012;37:1989–1991. Doi: 10.1364/OL.37.001989
[22] Gordon IE, Rothman LS, Hill C, Kochanov RV, Tan Y, Bernath PF, Birk M, Boudon V, Campargue A, Chance KV, Drouin BJ, Flaud JM, Gamache RR, Hodges JT, Jacquemart D, Perevalov, VI, Perrin A, Shine KP, Smith MAH, Tennyson J, Toon GC, Tran H, Tyuterev VG, Barbe A, Császár, AG, Devi VM, Furtenbacher T, Harrison JJ, Hartmann J-M, Jolly A, Johnson TJ, Karman T, Kleiner, I, Kyuberis AA, Loos J, Lyulin OM, Massie ST, Mikhailenko SN, Moazzen-Ahmadi N, Müller HSP, Naumenko OV, Nikitin AV, Polyansky OL, Rey M, Rotger M, Sharpe SW, Sung K, Starikova E, Tashkun SA, Vander Auwera J, Wagner G, Wilzewski J, Wcisło P, Yu S, Zak EJ. The HITRAN2016 Molecular Spectroscopic Database. J Quant Spectrosc Radiat Transf 2017;203:3-69. doi: 10.1016/j.jqsrt.2017.06.038.
[23] Kerstel ERT, Iannone RQ, Chenevier M, Kassi S, H-J Jost, Romanini D. A water isotope (^2H, ^{17}O, and ^{18}O) spectrometer based on optical feedback cavity-enhanced absorption for in situ airborne applications. Appl Phys B 2006;85:397–406. Doi: 10.1007/s00340-006-2356-1
[24] See the following link for more details: https://cetiat.fr/en/calibration
[25] A. Wexler. Vapor Pressure Formulation for Water in Range 0 to 100 °C. A Revision J Res Natl Bur Stand Sect. A 1976;80A:775-785. Doi: 10.6028/jres.080A.071
[26] A. Wexler. Vapor Pressure Formulation for Ice. J Res Natl Bur Stand, Sect. A 1977;81A:5-20.
[27] Hyland RW. A Correlation for the Second Interaction Virial Coefficients and Enhancement Factors for Moist Air. J Res Natl Bur Stand, Sect. A 1975;79A:551-60. Doi: 10.6028/jres.079A.017
[28] Hyland RW, Wexler A. Formulations for the thermodynamic properties of dry air from 173.15 K to 473.15 K, and of saturated moist air from 173.15 K to 372.15 K, at pressures to 5 MPa. ASHRAE Trans 1983;89:520-35.
[29] Thalman R, Zarzana K, Tolbert MA, Volkamer R. Rayleigh scattering cross-section measurements of nitrogen, argon, oxygen and air. J Quant Spectrosc Radiat Transf 2014;147:171–7. Doi: 10.1016/j.jqsrt.2014.05.030
[30] Thalman R, Zarzana KJ, Tolbert MA, Volkamer R. J Quant Spectrosc Radiat Transf 2017;189:281–2.
[31] Ptashnik IV, McPheat RA, Shine KP, Smith KM, Williams RG. Water vapor self-continuum absorption in near-infrared windows derived from laboratory measurements. J Geophys Res 2011;116:D16305. Doi: 10.1029/2011JD015603.
[32] Brown LR, Humphrey CM, Gamach RR. CO_2 broadened water in the pure rotation and v_2 fundamental regions. J Mol Spectrosc 2007;246:1–21. Doi : 10.1016/j.jms.2007.07.010
[33] Mikhailenko SN, Kassi S, Mondelain D, Gamache RR, Campargue A. A spectroscopic database for water vapor between 5850 and 8340cm^{-1}. J Quant Spectrosc Radiat Transf 2016;179:198-216. Doi 10.1016/j.jqsrt.2016.03.035.
[34] Campargue A, Kassi S, Mondelain D, Vasilchenko S, Romanini D. Accurate laboratory determination of the near infrared water vapor self-continuum: A test of the MT_CKD model. J Geophys Res Atmos 2016;121:13,180–203. doi:10.1002/2016JD025531
[35] Mondelain D, Vasilchenko S, Čermák P, Kassi S, Campargue A. The self- and foreign-absorption continua of water vapor by cavity ring-down spectroscopy near 2.35 µm. Phys Chem Chem Phys 2015;17:17762-17770. Doi: 10.1039/c5cp01238d
[36] Fleurbaey H, Mondelain D, Grilli R, Campargue A. Measurements of the water vapor continuum absorption by OFCEAS at 3.50 µm and 2.32 µm. (Accepted in J Quant Spectrosc Radiat Transf).
[37] Tonkov MV, Filippov NN, Bertsev VV, Bouanich JP, Nguyen Van Thanh, Brodbeck C, Hartmann J-M, Boulet C, Thibault F, Le Doucen R. Measurements and empirical modelling of pure CO_2 absorption in the 2.3 µm region at room temperature: far wings, allowed and collision-induced bands. Appl Opt 1996;35:4863–70.
[38] Hartmann J-M, Boulet C, Tran DD, Tran H, Baranov Y. Effect of humidity on the absorption continua of CO_2 and N_2 near 4 µm: Calculations, comparisons with measurements, and consequences for atmospheric spectra. J Chem Phys 2018;148:054304. Doi : 10.1063/1.5019994

[39] Hartmann J-M, Boulet C, Jacquemart D. Molecular dynamics simulations for CO_2 spectra. II. The far infrared collision-induced absorption band. J Chem Phys 2011 ;134:094316. doi:10.1063/1.3557681
[40] Hartmann J-M, Boulet C. Molecular dynamics simulations for CO_2 spectra. III. Permanent and collision-induced tensors contributions to light absorption and scattering. J Chem Phys 2011;134: 184312. doi:10.1063/1.3589143
[41] Hartmann J-M, Boulet C, Robert D, Chapter V - The far wings (beyond the impact approximation),, Editor(s): J-M Hartmann, C Boulet, D Robert, Collisional Effects on Molecular Spectra (Second Edition), Elsevier, 2021, Pages 291-335, https://doi.org/10.1016/B978-0-12-822364-2.00001-5.
[42] Pavlyuchko AI, Orlinson BS, Vigasin AA (2003) Variational Solution of Anharmonic Vibrational Problems for Polyatomics and Molecular Pairs. In: Camy-Peyret C, Vigasin AA (eds) Weakly Interacting Molecular Pairs: Unconventional Absorbers of Radiation in the Atmosphere. NATO Science Series (Series IV: Earth and Environmental Sciences), vol 27. Springer, Dordrecht. doi:10.1007/978-94-010-0025-3_5